Characterization of the axial plasma shock in a table top plasma focus after the pinch and its possible application to testing materials for fusion reactors

Leopoldo Soto, Cristian Pavez, José Moreno, María José Inestrosa-Izurieta, Felipe Veloso, Gonzalo Gutiérrez, Julio Vergara, Alejandro Clausse, Horacio Bruzzone, Fermín Castillo, and Luis F. Delgado-Aparicio

Citation: Physics of Plasmas (1994-present) **21**, 122703 (2014); doi: 10.1063/1.4903471
View online: http://dx.doi.org/10.1063/1.4903471
View Table of Contents: http://scitation.aip.org/content/aip/journal/pop/21/12?ver=pdfcov
Published by the AIP Publishing

Characterization of the axial plasma shock in a table top plasma focus after the pinch and its possible application to testing materials for fusion reactors

Leopoldo Soto,[1,2,3,a)] Cristian Pavez,[1,2,3] José Moreno,[1,2,3] María José Inestrosa-Izurieta,[1,2] Felipe Veloso,[4] Gonzalo Gutiérrez,[5] Julio Vergara,[6] Alejandro Clausse,[7] Horacio Bruzzone,[8] Fermín Castillo,[9] and Luis F. Delgado-Aparicio[10]
[1]*Comisión Chilena de Energía Nuclear, Casilla 188-D, Santiago, Chile*
[2]*Centro de Investigación y Aplicaciones en Física de Plasmas y Potencia Pulsada, P*^{4}*, Santiago-Talca, Chile*
[3]*Departamento de Ciencias Físicas, Facultad de Ciencias Exactas, Universidad Andrés Bello, República 220, Santiago, Chile*
[4]*Instituto de Física, Pontificia Universidad Católica de Chile, Santiago, Chile*
[5]*Departamento de Física, Facultad de Ciencias, Universidad de Chile, Santiago, Chile*
[6]*Facultad de Ingeniería, Pontificia Universidad Católica de Chile, Santiago, Chile*
[7]*CNEA-CONICET and Universidad Nacional del Centro, 7000 Tandil, Argentina*
[8]*CONICET and Universidad de Mar del Plata, Mar del Plata, Argentina*
[9]*Instituto de Ciencias Físicas, Universidad Nacional Autónoma de México, Cuernavaca, Morelos, Mexico*
[10]*Princeton Plasma Physics Laboratory, Princeton University, Princeton, New Jersey 08543, USA*

(Received 19 September 2014; accepted 20 November 2014; published online 5 December 2014)

The characterization of plasma bursts produced after the pinch phase in a plasma focus of hundreds of joules, using pulsed optical refractive techniques, is presented. A pulsed Nd-YAG laser at 532 nm and 8 ns FWHM pulse duration was used to obtain Schlieren images at different times of the plasma dynamics. The energy, interaction time with a target, and power flux of the plasma burst were assessed, providing useful information for the application of plasma focus devices for studying the effects of fusion-relevant pulses on material targets. In particular, it was found that damage factors on targets of the order of 10^4 $(W/cm^2)s^{1/2}$ can be obtained with a small plasma focus operating at hundred joules. © *2014 AIP Publishing LLC*.
[http://dx.doi.org/10.1063/1.4903471]

INTRODUCTION

An important issue still unsolved in the research applied to the production of controlled fusion energy is the characterization, testing, and development of advanced plasma facing materials capable of resisting the extreme radiation and heat loads expected in both fusion reactors and plasma chambers of high energy density plasmas. This goal calls for the fundamental understanding of plasma-wall interaction processes and the associated radiation effects on materials and components, occurring in the mainstream fusion devices such as Tokamaks and inertial confinement facilities, in which plasma simulators used in close connection with material characterization, as well as modelling activities play an important role.[1,2]

A Plasma Focus (PF) is a kind of pinch discharge in which a high-pulsed voltage is applied to a low-pressure gas, few millibar, between coaxial cylindrical electrodes, generating a short-duration high-density plasma region in the axis (pinch). PF pinches produce radiation pulses (neutrons and x-rays), shock waves, ions and electron beams, plasma filaments, plasma jets, and plasma bursts,[3–5] being an interesting plasma accelerator to study the effects of fusion-relevant pulses on materials. In effect, targets of different materials relevant to fusion reactors can be characterized using the PF environment (using single pulses, or several cumulative pulses), which can simulate conditions similar to those that will be encountered in larger fusion facilities. In this direction, materials test under intense pulse of fast ion beams and plasma streams have been conducted in a few experiments on large plasma focus facilities.[6,7] Therefore, the characterization of the plasma shock and radiation that would arrive on the sample targets is a necessary first step in this matter. The main products conveyed by PF discharges are neutrons and x-rays pulses, ion beams, plasma shocks, and jets. The neutron yield, x-ray production, and ion beams have been widely studied; however, no special attention has been given to the plasma dynamics after the pinch, or at least not with enough details.

In this article, a noninvasive characterization of the axial plasma shock in a small plasma focus after the pinch is presented. The experiments were carried out in a hundred joules PF device, PF-400J.[8,9] A pulsed Nd-YAG laser at 532 nm and 8 ns FWHM pulse duration was used to obtain Schlieren images at different times from the plasma dynamics, particularly after the pinch. The energy and timing of the plasma shock in the space suitable for the location of sample targets were assessed. Thus, the power, flux power density of the plasma shock, and the damage factor on a target were estimated.

EXPERIMENTS AND DIAGNOSTICS

The experiments were carried out in the PF-400 J[8] plasma focus ($C_0 = 880$ nF, $L_0 = 38$ nH, 30 kV charging voltage, 130 kA of peak current achieved in 300 ns from

[a)]lsoto@cchen.cl

400 J stored energy) using deuterium as working gas. The anode consists of a 12 mm diameter central copper cylinder partially covered by alumina at its base (21 mm insulator length). The effective length of the anode (free of insulation) is $Z_a = 7$ mm and it has a central hole of 3 mm radius. The cathode consists of a coaxial outer ring of 29 mm diameter made of eight copper rods uniformly spaced on the cathode base. All the experiments were performed at the optimum working pressure, 8–9 mbar of deuterium, producing $(1.2 \pm 0.2) \times 10^6$ neutrons per shot.[8,9]

The electrical circuit and plasma dynamics of a plasma focus discharge are schematically shown in Figure 1. The discharge is initiated by a high-voltage pulse applied between the electrodes through a spark-gap. The subsequent plasma dynamics shown in Fig. 1 is as follows: (I) the discharge starts over the insulator, (II) a plasma sheet is axially accelerated by Lorentz force, (III) arriving to the anode end the plasma starts to accelerate inward radially, (IV) and finally the sheet collapses in the axis to form a dense column of plasma (pinch). During this stage, ions beams, electron beams, hard X-rays, and fusion neutrons (if is operated in deuterium) are generated. After the pinch, the plasma column is ejected generating an axial plasma shock.

Electrical diagnostics. The voltage V(t) between electrodes was measured with a fast resistive divider located close to the discharge chamber and the current derivative dI(t)/dt was measured with a Rogowskii coil calibrated *in situ*. Figure 2 shows the electrical signals for a discharge at 9mbar charging at 28 kV.

Optical refractive diagnostics. In order to study the structure and dynamics of the plasma, Schlieren images were

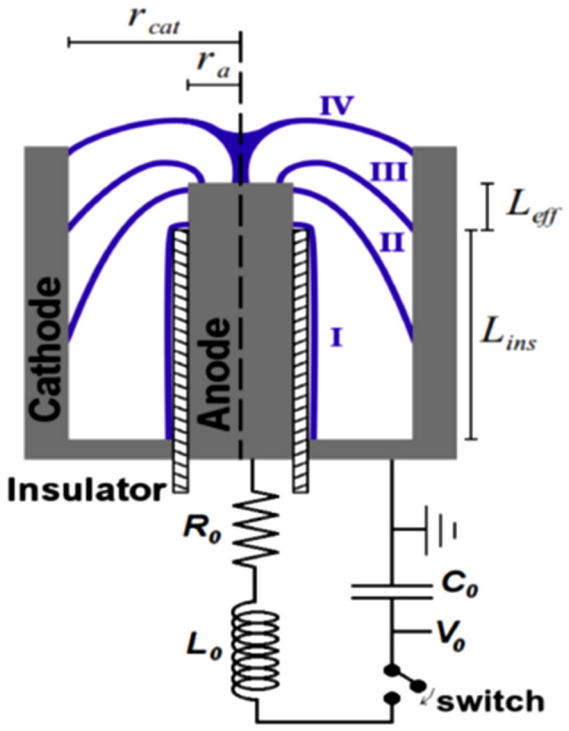

FIG. 1. Scheme of a plasma focus and its plasma dynamics. Cathode radius: r_{cat}, anode radius: r_a, effective anode length $L_{eff} = Z_a$, and insulator length: L_{ins}. Capacitance of the capacitor bank: C_0, charging voltage: V_0, total resistance: R_0, and total inductance: L_0.

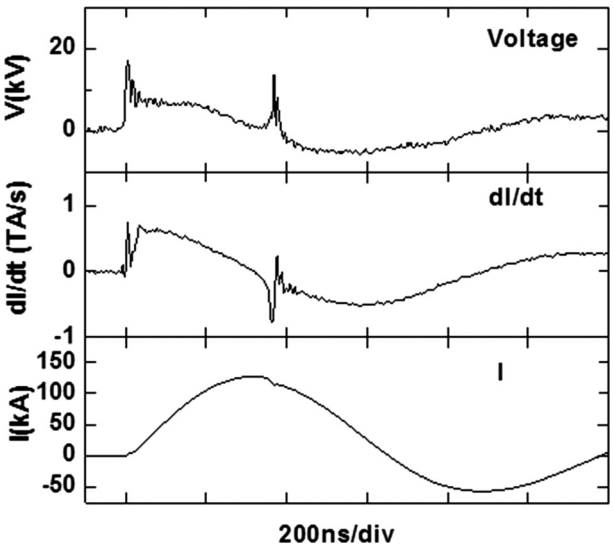

FIG. 2. Electrical signals for a shot in deuterium at 9 mbar, charging voltage = 28 kV. The typical dip in the signal of the current derivative associated with the formation of a pinched plasma column on the axis is clearly observed.

produced using a pulsed Nd-YAG laser (532 nm, 8 ns FWHM) synchronized with the discharge. The image acquisition was done using a digital camera with a CMOS size of 14.8 mm × 22.2 mm (5.2 μm pixel size). A regular bi-convex lens with a focal length of 25 cm and 5 cm of diameter was used to produce the image of the plasma on the CMOS. A pinhole of ~500 μm was used in the focal plane. A magnification $m = 0.52$ was used, thus one pixel corresponds to 10 μm. A resolution for the electron density gradient of the order $2.3 \times 10^{28}\,m^{-4}$ is obtained with the Schlieren system.

The global radial plasma dynamics of the PF-400J was previously studied with optical refractive diagnostics, including interferometry at pinch time.[10] In the radial phase, the plasma is compressed with a velocity of the order $(8 \pm 0.8) \times 10^4$ m/s forming a pinch plasma column with a radius of (1 ± 0.15)mm with a density on the axis of $(1 \pm 0.3) \times 10^{25}\,m^{-3}$, and the number of ions per unit length was $(8 \pm 1) \times 10^{18}\,m^{-1}$. Here, we report the observations and characterization of plasma bursts and axial plasma shock that appear after the pinch.

RESULTS

Figure 3 shows a sequence of the plasma dynamics from Schlieren images. The first two pictures correspond to the pinch formation. The following pictures correspond to the dynamics after the pinch ejection, which occurs close to $t \sim 20$ ns as seen from laser images. Note that while the pinch is ejected, a secondary axial plasma structure (bubble) intersecting the primary plasma appears. Figure 4 shows different fronts identified in the plasma structure. Z_1 indicates the rear of the axial plasma sheath, Z_2 is the front of the plasma sheath, and Z_3 is the axial front of a plasma bubble that appears after the pinch. Figure 5 shows the positions of Z_1, Z_2, and Z_3 at different times of the discharge ($t = 0$ corresponds to the time of the minimum value of the current derivative, i.e., close to the pinch time).

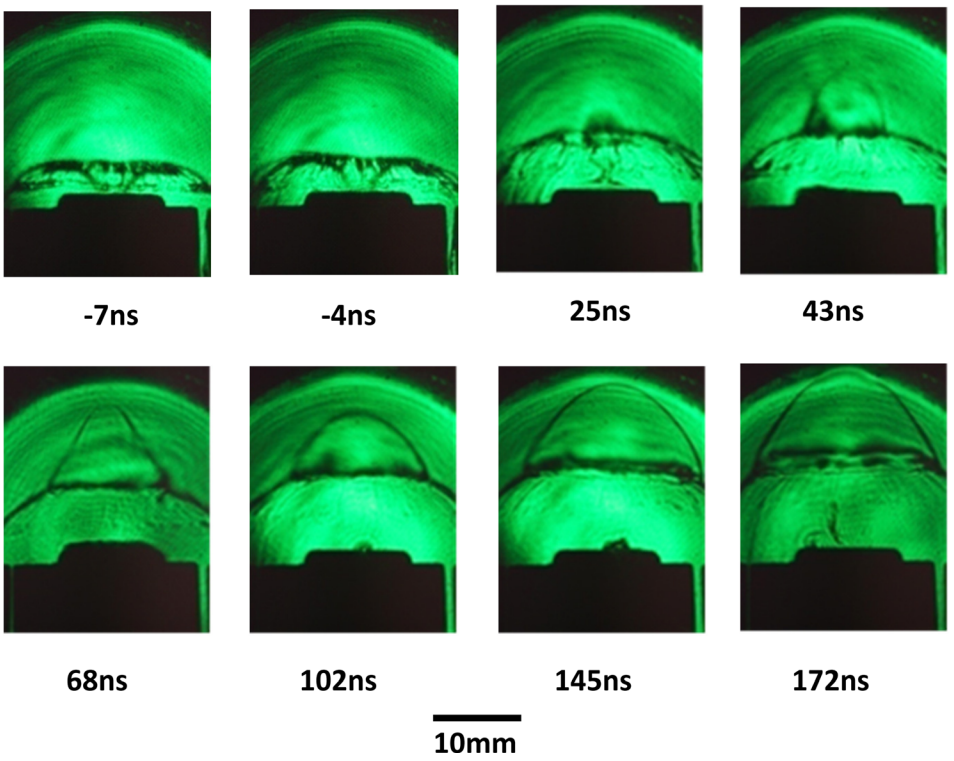

FIG. 3. Sequence of the plasma dynamics, Schlieren plasma images (t = 0 corresponds to the time of the minimum value of the current derivative, i.e., close to the pinch time). The first two pictures correspond to the pinch formation. The following pictures correspond to the dynamics after the pinch. Note that when the pinch is ejected (25 ns), a secondary intersecting bubble appears.

Plasma propagation. From Figure 5, it is possible to obtain the time-varying position of the fronts Z_1, Z_2, and Z_3. After the pinch, (i.e., $t > 20$ ns), both Z_1 and Z_2 show linear dependence with time, whereas Z_3 evolves differently. Z_1 and Z_2 plasma fronts move with constant average velocities $V_{Z1} = (3.0 \pm 0.2) \times 10^4$ m/s and $V_{Z2} = (3.4 \pm 0.2) \times 10^4$ m/s. This suggests that there are no net accelerations acting on them. The latter is consistent with the later stage of the current sheet rundown driven by the Lorentz force (see Eqs. (16) and (17) in Ref. 11 or 12), whose velocity approaches $V_Z \sim 0.8\, Z_a/(L_0\, C_0)^{1/2} = 3.1 \times 10^4$ m/s.

On the other hand, the Z_3 front evolution has a $t^{2/5}$ dependence (correlation coefficient $R^2 = 0.96$). This temporal dependence is consistent to the propagation of a strong shock freely propagating in a homogeneous atmosphere. An approximate assessment of the latter is[13]

$$Z_3(t) - Z_3(t_o) = \left[\frac{75}{16\pi}\frac{(\gamma-1)(1+\gamma)^2}{(3\gamma-1)}\frac{E}{\rho_o}\right]^{1/5}(t-t_o)^{2/5}, \quad (1)$$

where $Z_3(t)$ and $Z_3(t_o)$ are the plasma front position at times t and t_o, E is the energy responsible for the shock wave

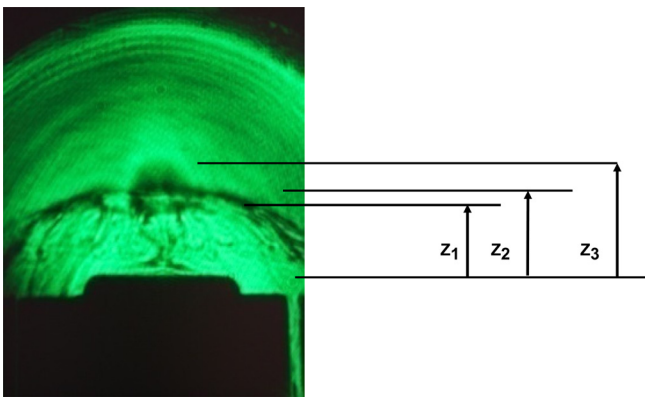

FIG. 4. Different fronts identified in the plasma structure. Z_1 indicates the rear of the axial plasma sheath, Z_2 is the front of the plasma sheath, and Z_3 is the axial front of a plasma bubble that appears after the pinch.

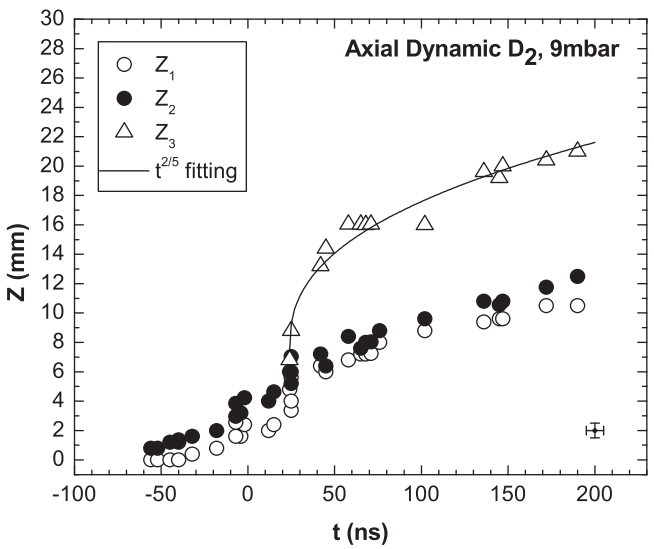

FIG. 5. Temporal evolution of the positions of the fronts Z_1, Z_2, and Z_3 obtained from several Schlieren plasma images as those shown in Figure 3 (t = 0 corresponds to the time of the minimum value of the current derivative, i.e., close to the pinch time). The error bar for the data is shown at 200 ns, 2 mm in the graph. The velocity of the rear axial plasma sheath Z_1 is $V_{Z1} = (3.0 \pm 0.2) \times 10^4$ m/s, between t = 60 ns and 190 ns. The velocity of the front axial plasma sheath Z_2 is $V_{Z2} = (3.4 \pm 0.2) \times 10^4$ m/s, between t = 60 ns and 190 ns. The axial velocity of the bubble front Z_3 is $V_{Z3} = (2.6 \pm 0.3) \times 10^5$ m/s, between t = 20 ns and 60 ns. Thus, from 60 ns to 190 ns the speed decreases to $V_{Z3} = (4.5 \pm 0.5) \times 10^4$ m/s.

formation at $t = t_o$, γ is the specific heat ratio of the back front, and ρ_o is the background mass density. According to the results shown in Fig. 5, Z_3 corresponds to a shock wave produced in $Z(t_o) = (7.6 \pm 0.6)$ mm over the anode surface at $t = t_o = 24$ ns (i.e., almost immediately after pinch). The curve shown in Fig. 5 corresponds to the fitting curve $Z_3(t) - Z_3(t_o) = (1.7 \pm 0.1)$ mm/ns$^{2/5}$(t − t$_0$)$^{2/5}$. The background gas is diatomic deuterium, whose density for the filling pressure and ambient temperature is 1.5×10^{-3} kg/m^3. Furthermore, according to the Hugoniot curves with dissociation and ionization (Sec. 9, Chap. 3, in Ref. 13), for plasma temperatures much larger than the dissociation and ionization energy of deuterium (∼14 eV) γ approaches 5/3. Hence, using Eq. (1), the energy responsible for the shock front Z_3 is $E = (12.5 \pm 3.5)$ J.

Conveyed mass. From the images, it is also possible to estimate roughly the total mass conveyed between Z_1 and Z_2 (m_{12}), which is the gas mass between the coaxial electrodes multiplied by the axial mass factor, f_m, i.e., the fraction of the mass that is moving within the plasma sheath in the coaxial gun.[12] For the present experimental conditions and using a snowplow model for the axial phase of a plasma focus,[12] f_m, was estimated in $f_m = 0.08$.[14] The volume in the coaxial plasma gun (gun length = 28 mm, external radius = 15.5 mm, internal radius = 6 mm) is 1.8×10^{-5} m^3. The number of atoms per volume at the filling pressure of 9 mbar is 4.86×10^{23} m^{-3}. Thus, the total mass swept in the axial phase is roughly: m_{12} = (volume in the plasma gun) × (number of atoms per volume at filling pressure) × (ion mass) × (f_m), $m_{12} \sim 2 \times 10^{-9}$ kg.

Mass ejected from the pinch. The mass ejected from the pinch, m_{23}, is effectively the mass producing the bubble, and can be estimated as the total mass of the pinch. The pinch density was previously measured using pulsed interferometry,[10] and the number of ions per unit length was estimated in 8×10^{18} m^{-1}, thus for a pinch of deuterium of 5.6 mm length, the total number of ions is 4.48×10^{16}, and the pinch mass is $m_{23} \sim 1.5 \times 10^{-10}$ kg. In addition, after the pinch ejection the plasma expands radially (roughly in a conical sector of a sphere due to the lateral confinement of the magnetic field and substantially no obstacles in the axis direction). Its thickness would roughly correspond to the pinch length, L ∼ 5.6 mm.

Kinetic energy of the axial plasma. In order to estimate the kinetic energy of the axial plasma after pinch, the average velocities of each plasma front can be used. For the Z_1 and Z_2 fronts, the estimated average velocity is close to 3.2×10^4 m/s. Since the mass of the interface has already been estimated ($m_{12} \sim 2 \times 10^{-9}$ kg), its corresponding kinetic energy is close to ∼1 J. For the case of the plasma shock Z_3 ($m_{23} \sim 1.5 \times 10^{-10}$ kg), two zones can be distinguished. One with an average initial velocity $\langle V_{Z3}\rangle_1$ $\sim 2.6 \times 10^5$ m/s (20 ns < t < 60 ns), resulting in a kinetic energy ∼ 5 J. Later when the velocity decreases to $\langle V_{Z3}\rangle_2 \sim 4.5 \times 10^4$ m/s (60 ns < t < 190 ns), the kinetic energy is ∼0.15 J.

Expected effects on material targets. For material test experiments, the plasma shock should impact actual targets, which can be placed in various locations depending on the expected effect. Two axial zones can be considered to locate a target: (a) close to the top of the pinch, where the velocity of the plasma shock Z_3 is $\langle V_{Z3}\rangle_1 \sim 2.6 \times 10^5$ m/s (i.e., between ∼9 and ∼16 mm from the anode top), and (b) where the velocity of Z_3 has decreased to $\langle V_{Z3}\rangle_2 \sim 4.5 \times 10^4$ m/s (i.e., between ∼16 and ∼20 mm from the anode top). The time interaction with the target is estimated by the plasma thickness divided by the average arriving velocity. An overall assessment of the expected plasma shock delivered on a material target located at these two positions from the anode top is shown in Tables I and II. The cross section, S, of the interaction of the plasma shock with the target was estimated from the images.

Note that, even though the time interaction of the plasma produced by PF devices is orders of magnitude shorter than the typical instruments used in radiation material tests (electron and ion beams, plasma accelerators), the power flux density is orders of magnitude higher than those instruments. In these conditions, many features of damage produced by plasma blasts, taking place in relatively long events, could be reproduced with small PF devices. In particular, in the projected tokamak ITER, energy loads in the divertor associated

TABLE I. Assessment of the magnitudes of the plasma shock delivered on a material target close to the top of the pinch, where the average velocity of the plasma shock Z_3 is $\langle V_{Z3}\rangle_1 \sim 2.6 \times 10^5$ m/s (i.e., between ∼9 and ∼16 mm from the anode top).

	Target located at 15 mm from the anode top	
	First shock	Second shock
Arriving time	∼50 ns	∼240 ns
Thickness	∼pinch length L ∼ 5.6 mm	$(Z_2\text{-}Z_1) \sim 2$ mm
Characteristic velocity	$\langle V_{Z3}\rangle_1 \sim 2.6 \times 10^5$ m/s	$V_{Z2} = (3.4 \pm 0.2)10^4$ m/s $V_{Z1} = (3.0 \pm 0.2)10^4$ m/s Mean velocity $\langle V\rangle \sim 3.2 \times 10^4$ m/s
Mass	$m_{23} \sim 1.5 \times 10^{-10}$ kg	$\sim 2 \times 10^{-9}$ kg
Kinetic energy, E	∼5 J	∼1 J
Time of interaction, τ	$\tau = L/\langle V_{Z3}\rangle_1 \sim 20$ ns	$\tau = (Z_2\text{-}Z_1) \times V_{Z1} \sim 60$ ns
Cross section estimated from the plasma images, S	S ∼ 2 cm^2	S ∼ 7 cm^2
Power flux density, $q = E/\tau S$	q ∼ 125 MW/cm^2	q ∼ 2.4 MW/cm^2
Integral damage factor, $F = q \cdot \tau^{1/2}$	F ∼ 1.8×10^4 (W/cm^2) s$^{1/2}$	F ∼ 5.9×10^2(W/cm^2) s$^{1/2}$
Pressure	$(m_{23}\langle V_{Z3}\rangle_1)/(\tau S) \sim 9.8 \times 10^6$ N/m^2	$(m_{12}\langle V\rangle)/(\tau S) \sim 1.5 \times 10^6$ N/m^2

TABLE II. Assessment of the plasma shock delivered on a material target far to the top of the pinch where the average velocity of the plasma shock Z_3 has decreased to $\langle V_{Z3}\rangle_2 \sim 4.5 \times 10^4$ m/s (i.e., between ~16 and ~20 mm from the anode top).

	Target located at 20 mm from the anode top	
	First shock	Second shock
Arriving time	~150 ns	>300 ns
Thickness	~pinch length L ~ 5.6 mm	$(Z_2\text{-}Z_1) \sim 2$ mm
Characteristic velocity	$\langle V_{Z3}\rangle_2 \sim 4.5 \times 10^4$ m/s	$V_{Z2} = (3.4 \pm 0.2)10^4$ m/s $V_{Z1} = (3.0 \pm 0.2)10^4$ m/s Mean velocity $\langle V\rangle \sim 3.2 \times 10^4$ m/s
Mass	$m_{23} \sim 1.5 \times 10^{-10}$ kg	$\sim 2 \times 10^{-9}$ kg
Kinetic energy, E	~0.15 J	~1 J
Time of interaction, τ	$\tau = L/\langle V_{Z3}\rangle_2 \sim 120$ ns	$\tau = (Z_2\text{-}Z_1) \times V_{Z1} \sim 60$ ns
Cross section estimated from the plasma images, S	$S \sim 3$ cm^2	$S > 7$ cm^2
Power flux density, $q = E/\tau S$	$q \sim 0.4$ MW/cm^2	$q < 2.4$ MW/cm^2
Integral damage factor, $F = q\cdot\tau^{1/2}$	$F \sim 1.4 \times 10^2$ (W/cm^2) s$^{1/2}$	$F < 5.9 \times 10^2$(W/cm^2) s$^{1/2}$
Pressure	$(m_{23}\langle V_{Z3}\rangle_1)/(\tau S) \sim 1.9 \times 10^5$ N/m^2	$(m_{12}\langle V\rangle)/(\tau S) \sim < 1.5 \times 10^6$ N/m^2

with the type I ELMs (edge localized modes) of the order of ~100 to 300 J/cm^2 are expected during $\tau \sim 0.1$–0.5 ms, with a number of pulses of $\sim 10^3$ per shot, with a frequency of the order of 0.5 to 2 Hz.[2,15] Thus, a power flux density $q \sim 1$ MW/cm^2 and a damage factor $F \sim q\cdot\tau^{1/2} \sim 10^4$(W/cm^2)s$^{1/2}$ are expected in ITER from type I ELMs. Remarkably, the same order of magnitude of the damage factor is obtained with the PF-400J. The latter is a remarkable finding: even though the neutron fluence produced by the table top plasma focus PF-400J at 15 mm from the anode top is too low to produce measurable effects on materials ($\sim 8 \times 10^4$ neutrons/cm^2 in 10 ns), the plasma ejected from the pinch produces a damage factor comparable to that expected by type I ELMs in ITER.

CONCLUSIONS

The axial plasma dynamics after the pinch was observed by means of Schlieren images in a plasma focus operating at hundreds of joules. Two phenomena can be distinguished: (i) A shock plasma wave appearing almost immediately after pinch, produced by the plasma ejected from the pinch ~7.6 mm over the anode surface. Given the location of the production of this plasma shock and its propagation away from pinch position, it does not ablate or erode the electrodes surfaces. Hence, no additional contamination of electrode material will be produced by this strong shock. Fitting the evolution of the axial shock with Eq. (1), it was found that the energy responsible for the shock front is $E = (12.5 \pm 3.5)$ J. Assuming that this energy comes from the pinch, it is possible to estimate the lower bound of the pinch temperature T. In effect, since E/ion = 3/2 kT and the total number of ions in the pinch is 4.48×10^{16}, thus the lower bound of the pinch temperature can be estimated in ~1.1 keV.

Two velocity zones can be distinguished for this shock. At early times, the average velocity of this shock is $\sim 2.6 \times 10^5$ m/s, with a corresponding kinetic energy of ~5 J (in the 20 ns < t < 60 ns range). At later times (60 ns to 190 ns after the pinch), the average velocity of the shock decreases to $\sim 4.5 \times 10^4$ m/s. (ii) Moreover, a secondary plasma front formed by the plasma swept in the coaxial run of the current sheet was observed. The thickness and velocity of this front are ~1 to 2 mm and $\sim 3.2 \times 10^4$ m/s. The corresponding mass and kinetic energy are $\sim 2 \times 10^{-9}$ kg and 1 J.

The expected effects of the plasma shock produced by a PF discharge on material targets will depend highly of the location of the target. Two regions on the axis can be clearly distinguished: (a) between ~9 mm and ~16 mm above the anode top (i.e., $\sim 1.5 < Z/a < 2.7$, with Z/a being the ratio between the distance from the anode top and the anode radius), where the average velocity of the plasma shock from the pinch is $\sim 2.6 \times 10^5$ m/s, and (b) between ~16 and ~20 mm from the anode top (i.e., $\sim 2.7 < Z/a < 3.5$) where the velocity of the plasma shock from the pinch has decreased to $\sim 4.5 \times 10^4$ m/s. In the region (a), power fluxes about 125 MW/cm^2 can be expected during interaction times around 20 ns; the corresponding damage factor $F \sim q\cdot\tau^{1/2}$ is $F \sim 1.8 \times 10^4$ (W/cm^2) s$^{1/2}$. This figures should be compared with the power flux conveyed in the run down, which is about 2.4 MW/cm^2 and the interaction time $\tau \sim 60$ ns, corresponding to $F \sim 5.9 \times 10^2$ (W/cm^2) s$^{1/2}$. Thus, in region (a) the expected effects from the plasma-bubble shock are 30 times greater than those expected from the plasma swept in the coaxial gun. Likewise, in region (b) the expected power flux is about 0.4 MW/cm^2 and the interaction time $\tau \sim 120$ ns corresponding to a damage factor $F \sim 1.4 \times 10^2$ (W/cm^2) s$^{1/2}$. Likewise, for the plasma swept by the axial phase in the gun, the expected power flux density is $q < 2.4$ W/cm^2 and the interaction time $\tau > 60$ ns; thus, the corresponding damage factor is $F \sim 5.9 \times 10^2$ (W/cm^2) s$^{1/2}$. Therefore, in this region, farther from the anode top, the expected energy flux can be attributed in 20% to the plasma bubble and 80% to the axial plasma shock from the gun. In this approach, the cross section, S, of the interaction of the plasma shock with the target was estimated from the images. An experimental measurement of S would give a value with more accuracy for the power flux and for the damage factor.

In summary, in the region close to the end of the pinch, the damage factor obtained with the PF-400 J is $F \sim 1.8 \times 10^4$ (W/cm^2) s$^{1/2}$, which is within the order of magnitude than the expected value for ITER ELMs type I ($F \sim 10^4$(W/cm^2) s$^{1/2}$). Therefore, the information obtained in this

experiment and analysis is useful to design experiments using the plasma focus PF-400J, or similar small plasma foci, as plasma accelerator, to study the effects of fusion-relevant cumulative pulses on target materials. For this application, the target should be located close to the end of the pinch, where the damage factor is of the order of $F \sim 10^4$ (W/cm^2) $s^{1/2}$ (i.e., as near as possible without affecting the initiation of the discharge and the radial plasma focus dynamics). In a plasma focus device, the damage factor could be tuning adjusting the axial position of the target. In addition, exposition frequencies of 1 Hz or greater can be obtained in small PF devices of hundred joules, like PF-400J, and thousand shots can be produced in few minutes. Therefore, important progresses could be achieved in materials testing for fusion reactors using small plasma focus devices as plasma sources. Planned experiments for testing materials as tungsten, molybdenum, among others, are currently on their way at the Chilean Nuclear Energy Commission using the PF-400J device.

ACKNOWLEDGMENTS

This work was supported by IAEA-CRP contract 16996, bilateral project CONICYT Chile–ANPCyT Argentina: CONICYT ACE-01, ANPCyT-PICT-2697, and CONICYT grant ACT-1115. The visit of F. Castillo to Chile was supported by FONDECYT grant 1110940. M. J. Inestrosa-Izurieta is supported by CONICYT-PAI grant 79130026.

[1]R. Kamendje *et al*., "Investigations of materials under high repetition and intense fusion-relevant pulses," in Summary of the 1st Research Coordination Meeting of the IAEA-CRP, 6-9 December 2011, Vienna, Austria, Paper No. F1.30.13.
[2]G. Federici, C. H. Skinner, J. N. Brooks, J. P. Coad, C. Grisolia, A. A. Haasz, A. Hassanein, V. Philipps, C. S. Pitcher, J. Roth, W. R. Wampler, and D. G. Whyte, Nucl. Fusion **41**(12R), 1967–2137 (2001).
[3]L. Soto, Plasma Phys. Controlled Fusion **47**, A361 (2005).
[4]L. Soto, C. Pavez, A. Tarifeño, J. Moreno, and F. Veloso, Plasma Sources Sci. Technol. **19**, 055017 (2010).
[5]L. Soto, C. Pavez, F. Castillo, F. Veloso, J. Moreno, and S. K. H. Auluck, Phys. Plasmas **21**, 072702 (2014).
[6]V. A. Gribkov, V. N. Pimenov, L. I. Ivanov, E. V. Dyomina, S. A. Maslyaev, R. Miklaszewski, M. Scholz, U. E. Ugaste, A. V. Dubrovsky, V. C. Kulikauskas, and V. V. Zatekin, J. Phys. D: Appl. Phys. **36**, 1817–1825 (2003).
[7]V. N. Pimenov, E. V. Demina, S. A. Maslyaev, L. I. Ivanov, V. A. Gribkov, A. V. Dubrovsky, Ü. Ugaste, T. Laas, M. Scholz, R. Miklaszewski, B. Kolman, and A. Tartari, Nukleonika **53**, 111 (2008).
[8]P. Silva, J. Moreno, L. Soto, L. Birstein, R. Mayer, and W. Kies, Appl. Phys. Lett. **83**, 3269 (2003).
[9]F. Veloso, C. Pavez, J. Moreno, V. Galaz, M. Zambra, and L. Soto, J. Fusion Energy **31**, 30–37 (2012).
[10]C. Pavez and L. Soto, Phys. Scr. **T131**, 014030 (2008).
[11]C. Moreno, H. Bruzzone, J. Martínez, and A. Clausse, IEEE Trans. Plasma Sci. **28**, 1735–1741 (2000).
[12]S. Lee, J. Fusion Energy **33**, 319 (2014).
[13]Y. Zel'dovich and Y. Raizer, *Physics of Shock Waves and High Temperature Phenomena* (Dover Publications Inc, New York, 2002).
[14]S. Lee, S. H. Saw, L. Soto, S. V. Springham, and S. P. Moo, Plasma Phys. Controlled Fusion **51**, 075006 (2009).
[15]I. E. Garkusha, A. N. Bandura, O. V. Byrka, V. V. Chebotarev, I. Landman, V. A. Makhlaj, S. Pestchanyi, and V. I. Tereshin, J. Nucl. Mater. **386–388**, 127–131 (2009).